

NO-A179 927

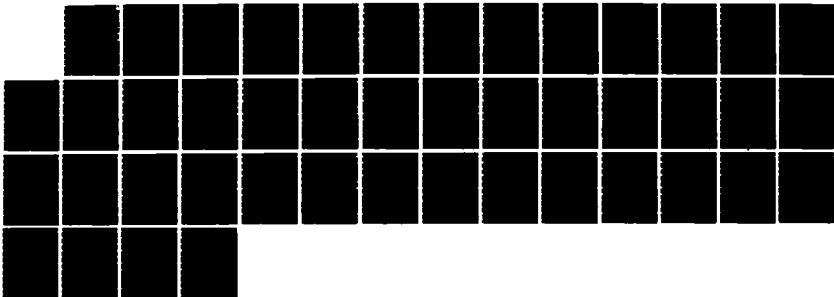
TWO-TONE INTERMODULATION IN DIODE MIXERS(U) AEROSPACE  
CORP EL SEGUNDO CA ELECTRONICS RESEARCH LAB S A MAAS  
30 SEP 86 TR-0086(6925-02)-5 SD-TR-87-14  
F04701-85-C-0086

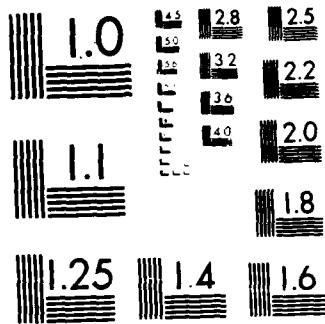
1/1

UNCLASSIFIED

F/G 9/1

NL





MICROCOPY RESOLUTION TEST CHART  
NATIONAL BUREAU OF STANDARDS-1963-A

12

AD-A179 927

# Two-Tone Intermodulation in Diode Mixers

S. A. MAAS  
Electronics Research Laboratory  
Laboratory Operations  
The Aerospace Corporation  
El Segundo, CA 90245

30 September 1986

Prepared for  
SPACE DIVISION  
AIR FORCE SYSTEMS COMMAND  
Los Angeles Air Force Station  
P.O. Box 92960, Worldway Postal Center  
Los Angeles, CA 90009-2960

DTIC  
ELICITE  
MAY 04 1987  
E

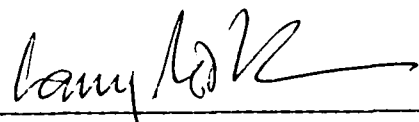
APPROVED FOR PUBLIC RELEASE  
DISTRIBUTION UNLIMITED

This report was submitted by The Aerospace Corporation, El Segundo, CA 90245, under Contract No. F04701-85-C-0086 with the Space Division, P. O. Box 92960, Worldway Postal Center, Los Angeles, CA 90009-2960. It was reviewed and approved for The Aerospace Corporation by M. J. Daugherty, Director, Electronics Research Laboratory.

Lt Larry H. North, Space Division/CWX, was the project officer for the Mission-Oriented Investigation and Experimentation (MOIE) Program.

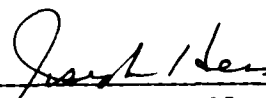
This report has been reviewed by the Public Affairs Office (PAS) and is releasable to the National Technical Information Service (NTIS). At NTIS, it will be available to the general public, including foreign nationals.

This technical report has been reviewed and is approved for publication. Publication of this report does not constitute Air Force approval of the report's findings or conclusions. It is published only for the exchange and stimulation of ideas.



---

LARRY H. NORTH, Lt, USAF  
MOIE Project Officer  
SD/CWX



---

JOSEPH HESS, GM-15  
Director, AFSTC West Coast Office  
AFSTC/WCO OL-AB

UNCLASSIFIED

SECURITY CLASSIFICATION OF THIS PAGE (When Data Entered)

REPORT DOCUMENTATION PAGE		READ INSTRUCTIONS BEFORE COMPLETING FORM
1. REPORT NUMBER SD-TR- 87-14	2. GOVT ACCESSION NO. ADP 179 937	3. RECIPIENT'S CATALOG NUMBER
4. TITLE (and Subtitle) TWO-TONE INTERMODULATION IN DIODE MIXERS		5. TYPE OF REPORT & PERIOD COVERED
7. AUTHOR(s) Stephen A. Maas		6. PERFORMING ORG. REPORT NUMBER TR-0086(6925-02)-5
9. PERFORMING ORGANIZATION NAME AND ADDRESS The Aerospace Corporation El Segundo, Calif. 90245		8. CONTRACT OR GRANT NUMBER(s) FO4701-85-C-0086
11. CONTROLLING OFFICE NAME AND ADDRESS Space Division Los Angeles Air Force Station Los Angeles, Calif. 90009-2960		10. PROGRAM ELEMENT, PROJECT, TASK AREA & WORK UNIT NUMBERS
14. MONITORING AGENCY NAME & ADDRESS (if different from Controlling Office)		12. REPORT DATE 30 September 1986
		13. NUMBER OF PAGES 41
		15. SECURITY CLASS. (of this report) Unclassified
		15a. DECLASSIFICATION/DOWNGRADING SCHEDULE
16. DISTRIBUTION STATEMENT (of this Report)  Approved for public release; distribution unlimited.		
17. DISTRIBUTION STATEMENT (of the abstract entered in Block 20, if different from Report)		
18. SUPPLEMENTARY NOTES		
19. KEY WORDS (Continue on reverse side if necessary and identify by block number) Dynamic range Intermodulation distortion Mixers Receivers		
20. ABSTRACT (Continue on reverse side if necessary and identify by block number) This report explores, experimentally and theoretically, the problem of minimizing second- and third-order intermodulation distortion in diode mixers. A numerical technique is presented which can be used to calculate intermodulation levels with unprecedented accuracy, and it is used to identify circuit and diode parameters which maximize dynamic range. It is shown that intermodulation distortion is minimized by using low diode junction capacitance and series resistance, short-circuit embedding		

DD FORM 1473  
(FACSIMILE)

UNCLASSIFIED

SECURITY CLASSIFICATION OF THIS PAGE (When Data Entered)

UNCLASSIFIED

SECURITY CLASSIFICATION OF THIS PAGE(When Data Entered)

19. KEY WORDS (Continued)

20. ABSTRACT (Continued)

impedances, and high local oscillator level. It is also shown that certain conditions which may optimize conversion loss, such as image enhancement, may severely exacerbate intermodulation. The theory is applicable at RF levels below saturation.

UNCLASSIFIED

SECURITY CLASSIFICATION OF THIS PAGE(When Data Entered)

PREFACE

The author wishes to thank R. M. Gowin for assistance with the fabrication of the mixers, W. A. Garber for measuring the diode C/V characteristic, and M. McColl, W. A. Johnson, and F. L. Vernon for reading and commenting on this report.

Accession For	
NTIS GRA&I	<input checked="" type="checkbox"/>
DTIC TAB	<input type="checkbox"/>
Unannounced	<input type="checkbox"/>
Justification	
By _____	
Distribution/	
Availability Codes	
Dist	Avail and/or Special
A-1	



## CONTENTS

PREFACE.....	1
INTRODUCTION.....	7
THEORY.....	9
IMPLEMENTATION.....	23
RESULTS.....	24
CONCLUSIONS.....	38
REFERENCES.....	40



## FIGURES

1.	IF spectrum of the most significant intermodulation components.....	10
2.	Large-signal mixer equivalent circuit.....	12
3.	Small-signal mixer equivalent circuit.....	14
4.	Small-signal equivalent circuits for (a) first-order, (b) second-order, and (c) third-order IM products.....	17
5.	Measured and calculated conversion loss and third-order IM output levels for -20 dBm RF input per tone.....	26
6.	Measured and calculated second-order IM output levels for -20 dBm RF input per tone.....	27
7.	Measured and calculated conversion loss and IM levels as a function of dc bias voltage.....	28
8.	Conjugate-match conversion loss and third-order IM for baseline diode and circuit parameters, except for different sets of high-order LO and small-signal (including image) embedding impedances.....	30
9.	Second-order IM output levels for the same conditions as in Figure 8.....	31
10.	Conjugate-match conversion loss, IM levels, and noise temperature as a function of image termination reactance, for baseline diode and circuit parameters.....	33
11.	Conversion loss and IM level vs. dc diode current for fixed LO power and fixed bias voltage conditions, and baseline circuit parameters.....	34
12.	Conversion loss and IM level dependence on series resistance.....	36
13.	Conversion loss and IM level dependence on zero-voltage junction capacitance.....	37
14.	Conversion loss and IM level dependence on $\phi$ and $\eta$ .....	39

## Two-Tone Intermodulation

in

## Diode Mixers

### Introduction

Intermodulation (IM) distortion often defines the upper limit to the signal handling capability of a microwave receiver. It is particularly serious in broadband receivers designed for communications or spectral surveillance. In such receivers the mixer is often the major generator of intermodulation distortion, because its signal handling ability is relatively low. Furthermore, if preamplifier stages are used to achieve a low noise figure, the signal levels applied to the mixer are correspondingly large.

Diode mixers exhibit intermodulation phenomena which have never been explained satisfactorily, and the related problem of selecting diode and circuit parameters to minimize intermodulation has not been investigated. It has been known for many years that the IM output level of a mixer usually, but not always, decreases with an increase in LO level, and that nulls in the IM output level sometimes occur at specific values of LO level or dc bias. Beane [1] and Graham and Ehrman [2] explain why some of these phenomena occur, but do not explain why they sometimes do not. Similarly Lepoff and Cowley [3] and Tou and Chang [4] describe techniques to reduce IM distortion in mixers, but do not address the greater problems of analysis and design for minimal IM. This paper will present theory which reproduces these phenomena with high accuracy, and will identify diode

and circuit parameters which minimize mixer IM.

Many useful techniques for analyzing nonlinear circuits, such as the Volterra series, assume weak nonlinearities and relatively small applied voltages (i.e. a small-signal, quasi-linear assumption). Unfortunately, these assumptions are violated by diode mixers, which have a very strong exponential nonlinearity and one signal, the local oscillator (LO), which may be several orders of magnitude larger than the other signals. Even with techniques which do not require a small-signal quasi-linear assumption, such as that of Ushida and Chua [5], the presence of one signal much larger than the others may introduce numerical problems. One way to circumvent these problems is to treat the pumped diode as a time-varying, weakly nonlinear device. Orloff [6] follows this approach by expanding the junction voltage in a Taylor series, using the LO voltage as the central value, to analyze single-tone IM. Swerdlow [7] applies a time-varying Volterra series to the analysis of a varactor upconverter, assuming a sinusoidal LO current ("current-pumped") waveform. Graham and Ehrman also apply time-varying Volterra series techniques to mixers using lumped circuit elements. Several specialized analyses have been presented [8-10] which have various advantages and limitations. The problems with these are that they make implicit or explicit assumptions about the diode's embedding impedances or LO waveforms, do not include junction capacitance or series resistance, or are limited in the order of nonlinearity which can be considered. It will be shown that these factors are critical to mixer IM performance.

The analysis presented here is an extension of existing large-signal/small-

signal mixer theory [11], [12]. It requires no assumptions about the LO waveform, any embedding impedance at any mixing or intermodulation frequency can be specified, and both the junction capacitance and conductance nonlinearities are included. By accounting for all important parameters, unprecedented accuracy has been obtained. It is directly applicable to a wide variety of circuits such as varactor upconverters, subharmonic mixers, and many types of modulators, and the same techniques could be applied to FET mixers. Once the conventional mixer analysis is performed, no further iteration is required. It is efficient enough to be implemented on a small computer such as the IBM PC.

Because any multiple-diode mixer can be modeled by an equivalent single-diode mixer, it is generally applicable to balanced mixers. Its main limitation is that saturation effects are not included, and the RF level must be comfortably below saturation (i.e. 10 dB or more below the 1-dB compression point).

### Theory

Figure 1 shows the intermediate frequency (IF) spectrum of intermodulation frequencies of greatest concern, up to third order, for two input tones. Only the intermodulation frequencies at the IF are shown, although similar IM voltage and current spectra exist at frequencies above and below each LO harmonic.  $\omega_1$  and  $\omega_2$  are the desired IF outputs. The diode may have different embedding impedances at each of these frequencies.

The small-signal junction voltage can be treated as a small deviation of the large-signal LO voltage. Hence the IM current can be found by a Taylor series expansion using the LO voltage as a central "point," and a relatively small number of terms in the series are adequate. The resulting series coefficients are time-varying. The general approach is as follows:

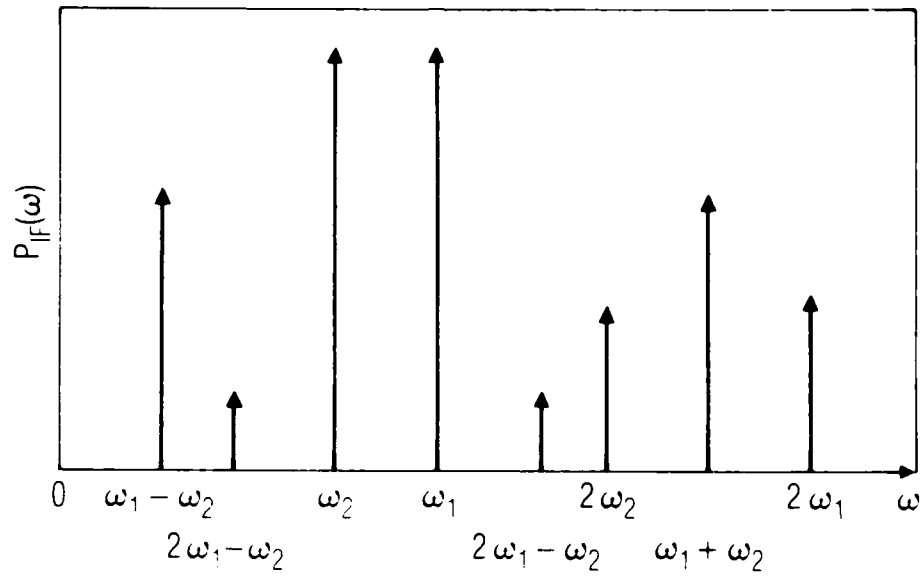


Fig. 1. IF spectrum of the most significant intermodulation components

1. Perform the large-signal analysis to determine the junction LO voltage and current waveforms;
2. Perform the linear time-varying small-signal analysis to determine the first-order junction voltages.
3. Use the first-order voltages as excitations to determine the second-order voltages.
4. Use the first- and second-order voltages to determine the third-order voltages.

Steps (1) and (2) are simply the conventional diode mixer analysis. The process could be continued for higher order IM components.

Figure 2 shows the large-signal equivalent circuit. The diode junction current  $I(V_j)$  and capacitive charge  $Q(V_j)$  are given by the well-known expressions

$$I_j(V_j) = I_0 \left[ \exp\left(\frac{qV_j}{\eta KT}\right) - 1 \right] \cong I_0 \exp(\delta V_j) \quad (1)$$

$$Q(V_j) = -2\phi C_{j0} \left(1 - \frac{V_j}{\phi}\right)^{1/2} \quad (2)$$

where  $I_0$  is the diode's reverse saturation current,  $C_{j0}$  is the zero-voltage junction capacitance, and  $\phi$  is the built-in voltage,  $q$  is the electron charge,  $K$  is Boltzmann's constant,  $T$  is absolute temperature, and  $\eta$  is the ideality factor. Eq. (2) implies that the epilayer doping is uniform.

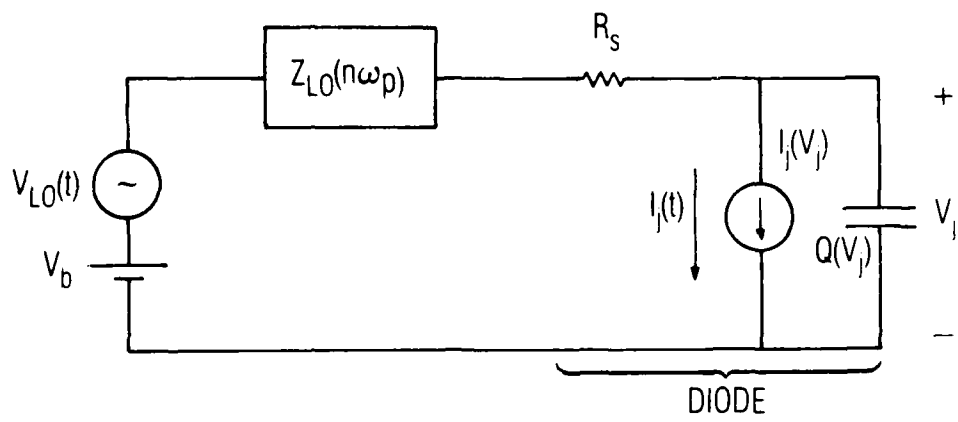


Fig. 2. Large-signal mixer equivalent circuit

The large signal analysis of the diode under LO excitation only is performed first, via any method which does not involve limiting assumptions (e.g. [13]). It is henceforth assumed that the LO waveforms  $I_j(t)$ ,  $V_j(t)$ , and  $C_j(t) = dQ(V)/dV$ ,  $V = V_j(t)$ , are known.

Figure 3 shows the small-signal equivalent circuit.  $i_s(t)$  is the Thevenin equivalent of the RF source, applied directly to the junction, and  $v_j(t)$  is the small-signal junction voltage, which includes the IM components and linear terms, but not the LO voltage. For two-tone distortion,

$$i_s(t) = I_{s1} \cos((m\omega_p + \omega_1)t) + I_{s2} \cos((m\omega_p + \omega_2)t) \quad (3)$$

where  $\omega_p$  is the LO fundamental frequency. Usually, but not necessarily,  $m=1$ , implying an upper-sideband RF input. The total junction voltage is  $V_j(t) + v_j(t)$ . Substituting this into (1) and (2) and expanding in a Taylor series about  $V_j(t)$  gives, for the small-signal junction current and charge,

$$i_j(t) = I_j(t) \left[ \delta v_j(t) + \delta^2 v_j^2(t)/2 + \delta^3 v_j^3(t)/6 + \dots \right] \quad (4)$$

$$q_j(t) = C_j(t) \left[ 2(\phi - V_j(t))v_j(t) + (\phi - V_j(t))^{-1}v_j^2(t)/4 + (\phi - V_j(t))^{-2}v_j^3(t)/8 + \dots \right] \quad (5)$$

Eqs. (4) and (5) can be expressed more generally as



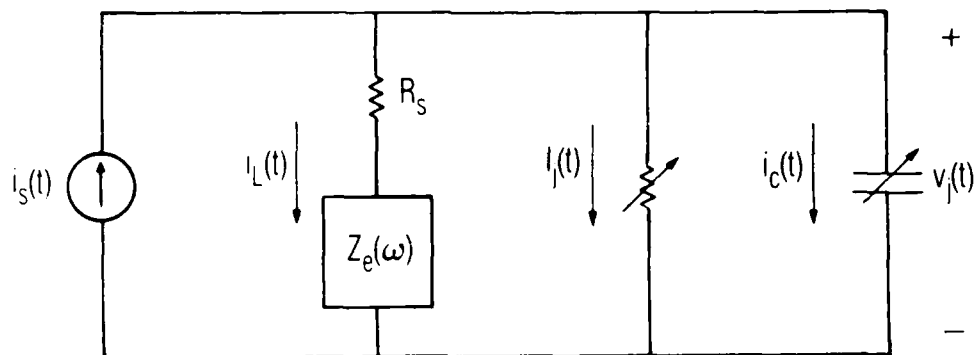


Fig. 3. Small-signal mixer equivalent circuit

$$i_j(t) = g_1(t)v_j(t) + g_2(t)v_j^2(t) + g_3(t)v_j^3(t) + \dots \quad (6)$$

$$q_j(t) = c_1(t)v_j(t) + c_2(t)v_j^2(t) + c_3(t)v_j^3(t) + \dots \quad (7)$$

Limiting consideration to third-order IM components,

$$v_j(t) = v_1(t) + v_2(t) + v_3(t) \quad (8)$$

$$v_j^2(t) = v_1^2(t) + 2v_1(t)v_2(t) \quad (9)$$

$$v_j^3(t) = v_1^3(t) \quad (10)$$

where  $v_n(t)$  is the  $n^{\text{th}}$  order IM voltage, the sum of the frequencies of any  $n$  first-order junction voltages. The differential equation describing Figure 3 is

$$\frac{dq_j(t)}{dt} + i_j(t) + i_L(t) = i_s(t) \quad (11)$$

Substituting (6) through (10) into (11) and separating gives the equations for first, second, and third-order products

$$\frac{d(c_1(t)v_1(t))}{dt} + g_1(t)v_1(t) + i_{L1}(t) = i_s(t) \quad (12)$$

$$\frac{d(c_1(t)v_2(t) + c_2(t)v_1^2(t))}{dt} + g_1(t)v_2(t) + g_2(t)v_1^2(t) + i_{L2}(t) = 0 \quad (13)$$

$$\begin{aligned} \frac{d}{dt}(c_1(t)v_3(t) + 2c_2(t)v_1(t)v_2(t) + c_3v_1^3(t)) + \\ g_1(t)v_3(t) + 2g_2(t)v_1(t)v_2(t) + g_3(t)v_1^3(t) + \\ i_{L3}(t) = 0 \end{aligned} \quad (14)$$

where  $I_{L1}$ ,  $I_{L2}$ , and  $I_{L3}$  are the first-, second-, and third-order load currents, respectively.

Figure 4(a), (b), and (c) show the first, second, and third-order equivalent circuits representing (12), (13), and (14), respectively. Figure 4(a) is the small-signal linear equivalent circuit. The voltages  $v_1(t)$  resulting from the two excitation tones can be found in the conventional manner. These are used to find the excitation currents, the sources in Figure 4(b), for the second order IM components (these sources are in fact the short-circuit junction IM currents). Given those currents, Figure 4(b) is a linear circuit so  $v_2(t)$  and  $i_{L2}(t)$  can be found by conversion matrix analysis in the same manner as  $i_{L1}(t)$  and  $v_1(t)$ . The third-order IM products are found analogously through the circuit in Figure 4(c).

The small-signal linear mixer analysis gives  $v_1(t)$ :

$$v_1(t) = \frac{1}{2} \sum_{m=-\infty}^{\infty} \sum_{\substack{q=-2 \\ q \neq 0}}^2 V_{m,q} \exp[j(m\omega_p + \omega_q)t] \quad (15)$$

so

$$v_1^2(t) = \frac{1}{4} \sum_{\substack{m \\ = -\infty}}^{\infty} \sum_{\substack{n \\ = -\infty}}^{\infty} \sum_{\substack{q \\ = -2 \\ q, r \neq 0}}^2 \sum_{\substack{r \\ = -2 \\ q, r \neq 0}}^2 V_{m,q} V_{n,r} \exp\{j[(m+n)\omega_p + \omega_q + \omega_r]t\} \quad (16)$$

The second-order terms of most interest are those at  $k\omega_p + \omega_1 - \omega_2$  and

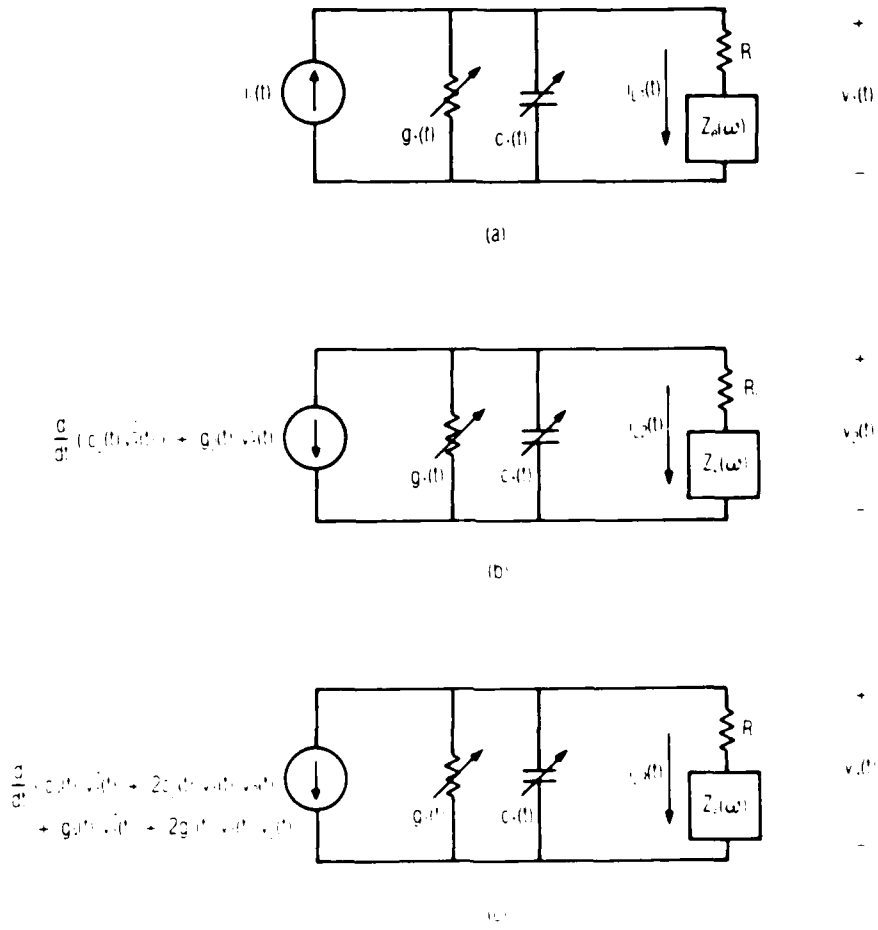


Fig. 4. Small-signal equivalent circuits for (a) first-order, (b) second-order, and (c) third-order IM products

$k\omega_p + 2\omega_1$ . These are the second-order IM frequencies most likely to cause interference, and are needed to find the third-order IM components. They will be designated by "a" and "b" subscripts, respectively. Then

$$v_{1a}^2(\tau) = \frac{1}{2} \sum_{m=-\infty}^{\infty} \sum_{n=-\infty}^{\infty} V_{m,1} V_{n,-2} \exp(j[(m+n)\omega_p + \omega_1 - \omega_2]\tau) \quad (17)$$

$$v_{1b}^2(\tau) = \frac{1}{4} \sum_{m=-\infty}^{\infty} \sum_{n=-\infty}^{\infty} V_{m,1} V_{n,1} \exp(j[(m+n)\omega_p + 2\omega_1]\tau) \quad (18)$$

The frequencies  $k\omega_p + \omega_1 + \omega_2$  may also be of concern; they can be found from (17) by replacing  $V_{n,-2}$  with  $V_{n,2}$  and following through the subsequent equations. Note also that (17) and (18), and the equations which follow from them, are sums of the upper-sideband phasor components at the relevant frequency, and not the complete time waveform. Eq. (17) has a coefficient of 1/2, instead of 1/4, because there are two identical terms in the q,r summation in (16). This situation arises frequently in the following equations.

The Taylor series coefficients can be expressed by their Fourier series' as

$$g_2(t) = \frac{\delta^2}{2} I_j(t) = \frac{\delta^2}{2} \sum_{l=-\infty}^{\infty} I_l \exp(jl\omega_p t) \quad (19)$$

$$c_2(t) = \frac{C_j(t)}{4(\phi - V_j(t))} = \sum_{l=-\infty}^{\infty} C_{2l} \exp(jl\omega_p t) \quad (20)$$

Using (17)-(20), Figure 4(a), and (13), the excitation current components are

$$i_{2a}(t) = \frac{1}{2} \sum_{l=-\infty}^{\infty} \sum_{m=-\infty}^{\infty} \sum_{n=-\infty}^{\infty} V_{m,1} V_{n,-2} \left( \frac{\delta^2}{2} I_l + C_{2l} \right) \exp(j[(1+m+n)\omega_p + \omega_1 - \omega_2]t) \quad (21)$$

$$i_{2b}(t) = \frac{1}{2} \sum_{l=-\infty}^{\infty} \sum_{m=-\infty}^{\infty} \sum_{n=-\infty}^{\infty} V_{m,1} V_{n,1} \left( \frac{\delta^2}{2} I_l + C_{2l} \right) \exp(j[(1+m+n)\omega_p + 2\omega_1]t) \quad (22)$$

$i_{2a}(t)$  and  $i_{2b}(t)$  are of the form

$$i_{2a}(t) = \frac{1}{2} \sum_{k=-\infty}^{\infty} I_{k,2a} \exp[j(k\omega_p + \omega_1 - \omega_2)t] \quad (23)$$

$$i_{2b}(t) = \frac{1}{2} \sum_{k=-\infty}^{\infty} I_{k,2b} \exp[j(k\omega_p + 2\omega_1)t] \quad (24)$$

Equating terms at the same frequency in (23)/(21) and (24)/(22), one obtains

$$I_{k,2a} = \sum_{l=-\infty}^{\infty} \sum_{m=-\infty}^{\infty} \sum_{n=-\infty}^{\infty} V_{m,1} V_{n,-2} \left( \frac{\delta^2}{2} I_1 + C_{21} j(k\omega_p + \omega_1 - \omega_2) \right) \quad (25)$$

$l+m+n = k$

$$I_{k,2b} = \frac{1}{2} \sum_{l=-\infty}^{\infty} \sum_{m=-\infty}^{\infty} \sum_{n=-\infty}^{\infty} V_{m,1} V_{n,1} \left( \frac{\delta^2}{2} I_1 + C_{21} j(k\omega_p + 2\omega_1) \right) \quad (26)$$

$l+m+n = k$

$k=l+m+n$  must be limited to some range  $(-K, K)$ ; then (25) and (26) can be expressed as column vectors of the form

$$\underline{I}_{2a} = (I_{-K,2a} \quad I_{-K+1,2a} \quad \dots \quad I_{-1,2a} \quad I_{0,2a} \quad I_{1,2a} \quad \dots \quad I_{K,2a})^T \quad (27)$$

and similarly for  $\underline{I}_{2b}$ .

The vectors of output IM currents,  $\underline{I}_{L2a}$  and  $\underline{I}_{L2b}$  are found from a straightforward conversion matrix analysis of Fig. 4b:

$$\underline{I}_{L2a} = (1 + \underline{Y}_j (\underline{Z}_{e2a} + R_s 1))^{-1} \underline{I}_{2a} \quad (28)$$

$$\underline{I}_{L2b} = (1 + \underline{Y}_j (\underline{Z}_{e2b} + R_s 1))^{-1} \underline{I}_{2b} \quad (29)$$

$\underline{Y}_j$  is the conversion matrix for the pumped diode junction [12].  $\underline{Z}_{e2a}$  and  $\underline{Z}_{e2b}$  are the  $2K+1 \times 2K+1$  diagonal matrices of embedding impedances at

the IM frequencies, with the impedances at  $K\omega_p + \omega_1 - \omega_2$  and  $K\omega_p + 2\omega_1$  at the top left corners, respectively.  $R_s$  is the diode series resistance. The second-order junction voltages are

$$V_{2a} = (Z_{e2a} + R_s) I_{L2a} \quad (30)$$

$$V_{2b} = (Z_{e2b} + R_s) I_{L2a} \quad (31)$$

and the second-order IM output powers at the IM frequencies near the  $k^{\text{th}}$  LO harmonic are

$$P_{k,2a} = 0.5 \left| I_{k,L2a} \right|^2 \text{Re}(Z_{e2a,k}) \quad (32)$$

$$P_{k,2b} = 0.5 \left| I_{k,L2b} \right|^2 \text{Re}(Z_{e2b,k}) \quad (33)$$

The third-order IM components are found analogously via (14) and Figure 4(c). The IM component of greatest interest is that at  $2\omega_1 - \omega_2$ , (or  $2\omega_2 - \omega_1$ , which is derived identically), since it usually can not be rejected by filters. The  $v_1(t)v_2(t)$  term in (14) has two components which generate  $2\omega_1 - \omega_2$ :  $v_1(t)$  at  $\omega_1$  mixing with  $v_{2a}(t)$  at  $\omega_1 - \omega_2$ , and  $v_1(t)$  at  $-\omega_2$  mixing with  $v_{2b}(t)$  at  $2\omega_1$ . The components of  $v_1^3(t)$  and  $v_1(t)v_2(t)$  at these frequencies are

$$v_1^3(t) = \frac{3}{8} \sum_m \sum_n \sum_p V_{m,1} V_{n,1} V_{p,-2} \exp(j\{(m+n+p)\omega_p + 2\omega_1 - \omega_2\}t) \quad (34)$$

Again, the coefficient is 3/8 instead of 1/8 because there are three identical terms in the q,r summation.



$$v_1(t)v_{2a}(t) = \frac{1}{4} \sum_{m=-\infty}^{\infty} \sum_n V_{m,2a} V_{n,1} \exp(j[(m+n)\omega_p + 2\omega_1 - \omega_2]t) \quad (35)$$

$$v_1(t)v_{2b}(t) = \frac{1}{4} \sum_{m=-\infty}^{\infty} \sum_n V_{m,2b} V_{n,-2} \exp(j[(m+n)\omega_p + 2\omega_1 - \omega_2]t) \quad (36)$$

The IM coefficients  $c_3(t)$  and  $g_3(t)$  are

$$c_3(t) = \sum_{l=-\infty}^{\infty} C_{3l} \exp(jl\omega_p t) \quad (37)$$

$$g_3(t) = \frac{\delta^3}{6} \sum_{l=-\infty}^{\infty} I_1 \exp(jl\omega_p t) \quad (38)$$

An analogous treatment for (14) gives the components of the third-order source and IM output current vectors:

$$\begin{aligned} I_{k,3} = & \frac{1}{4} \sum_l \sum_{m=-\infty}^{\infty} \sum_n \sum_p V_{m,1} V_{n,1} V_{p,-2} \left( \frac{\delta^3}{2} I_1 + \right. \\ & \left. 3C_{3l} j[k\omega_p + 2\omega_1 - \omega_2] \right) \\ & + \sum_l \sum_{m=-\infty}^{\infty} \sum_n (V_{m,2a} V_{n,1} + V_{m,2b} V_{n,-2}) \left( \frac{\delta^2}{2} I_1 + \right. \\ & \left. C_{2l} j[k\omega_p + 2\omega_1 - \omega_2] \right) \end{aligned} \quad (39)$$

$$\underline{I}_{L3} = (\underline{1} + \underline{Y}_j(\underline{Z}_{e3} + \underline{R}_s \underline{1})^{-1} \underline{I}_3 \quad (40)$$

where  $\underline{Z}_{e3}$  is the embedding impedance matrix at the third-order mixing frequencies and  $\underline{I}_3$  is the third-order source current column vector. The output IM power at  $k\omega_p + 2\omega_1 - \omega_2$  is

$$P_{k,3} = 0.5 \left| I_{k,L3} \right|^2 \operatorname{Re}(Z_{e3,k}) \quad (41)$$

### Implementation

The Turbo-Pascal [14] program DIODEMX listed in [12] was modified to include the IM calculations [15]. DIODEMX calculates the LO voltage, current, and capacitance waveforms,  $V_j(t)$ ,  $i_{LO}(t)$ , and  $C_j(t)$ , via a harmonic balance technique. It then forms conversion matrices for the junction and finds the first-order junction voltages,  $V_{m,\pm 1}$  and  $V_{n,\pm 2}$ . It also supplies the matrix  $\underline{Y}_j$  for Eqs. (28), (29), and (40). The evaluation of the multiple summations and determination of the IM output powers are then performed by a single new subroutine. Some economies in execution time are obtained by recognizing that many of the terms in the multiple summations are identical, and need not be evaluated repeatedly. Considering 12 LO harmonics in  $I_1$ ,  $C_{21}$ , and  $C_{31}$ , and nine mixing frequencies in the conversion matrices and in  $V_{m,\pm 1}$  and  $V_{n,\pm 2}$ , execution of the IM subroutine requires 49 seconds, using an IBM PC with an 8087 math coprocessor. Execution time is approximately half this value with an 80286-based microcomputer and 80287 numeric coprocessor.

The calculations can be simplified by the assumption that the two input tones are closely spaced in frequency, and that the IM outputs are within the IF passband. Under this assumption,  $V_{m,\pm 1} = V_{m,\pm 2}$ ,  $Z_{e3} = Z_{e2} = Z_{e1}$ , Eqs. (28), (29), and (40) are identical, and a large block of impedance data need not be entered. The validity of this assumption may be questionable in

certain cases only for either the  $2\omega_1$  or the  $\omega_1 - \omega_2$  component, one of which may be well separated from the other. In most cases the results are of acceptable accuracy even if the assumptions are not strictly valid. In situations where this approximation is not acceptable, one can enter the IF load impedances for these components individually.

### Results

The theory was verified experimentally with a single-ended mixer operating at approximately 10.5 GHz with an IF near 50 MHz. The sole purpose of the mixer was to verify the theory, not to achieve any performance goals; it was designed primarily to have predictable embedding impedances at as many LO harmonics and mixing frequencies as possible. The mixer consists of a diode mounted at the end of a 50 ohm microstrip line, with a 10 pF dc/IF blocking capacitor at the input and a decoupling circuit for dc bias and the IF output. LO and RF were applied through the input port via a directional coupler. Bias was applied through a bias tee in the IF circuit. The mixer was realized in microstrip on a 0.025" alumina substrate.

The diode was a silicon Schottky-barrier beam-lead device, Alpha model no. DML6777. Its parameters were  $R_s = 6.0 \Omega$ ,  $C_{j0} = 0.15$  pF,  $\phi = 0.7$  V,  $\eta = 1.19$ , and  $I_0 = 5.0 \times 10^{-12}$  A, determined by direct measurement of its C/V and I/V characteristics. The beam-lead overlay capacitance plus the calculated microstrip open-end capacitance was 0.10 pF. This capacitance in parallel with the 50 ohm source comprised the embedding network.

Figure 5 shows the measured and calculated conversion loss and third-order IM output level for -20 dBm input, with zero dc bias. The calculations include the effect of an estimated 0.5 dB input loss. Figure 6 shows the two second-order IM output levels under the same conditions. Figure 7 shows the measured and calculated dependence of conversion loss and IM upon dc bias voltage at a fixed LO level of 0 dBm. The agreement over a wide LO power range is remarkably good; in particular, the nulls in IM level at specific values of LO power and bias are faithfully reproduced.

Other mixer and diode parameters were examined to identify those which most strongly affect mixer IM performance. A set of baseline diode and circuit parameters was defined, and certain of these were varied while the rest were held fixed. The baseline parameter values were  $C_{j0} = 0.15$  pF,  $R_s = 9.0 \Omega$ ,  $\eta = 1.30$ ,  $\phi = 0.6$  V, and  $I_0 = 2.6 \times 10^{-9}$  A. The embedding impedances were zero at the image frequency, LO harmonics, and all high-order mixing frequencies. The LO fundamental source impedance was  $50 + j0 \Omega$ . In order to eliminate uncertainties due to source/load VSWR, all data was tabulated for simultaneously conjugate-matched RF and IF ports. This approach has the disadvantage that the conversion loss optimum often occurs at very low LO levels, sometimes with impractically high source/load impedances, and if the mixer is conditionally stable, a simultaneous conjugate match is impossible. For the most important cases of high LO level (i.e.  $\geq 3$  dBm), however, impedances are invariably reasonable and the mixer is stable. The RF frequencies were 10.54 and 10.56 GHz and the LO frequency was 10.50 GHz. The RF input level was -20 dBm per tone.

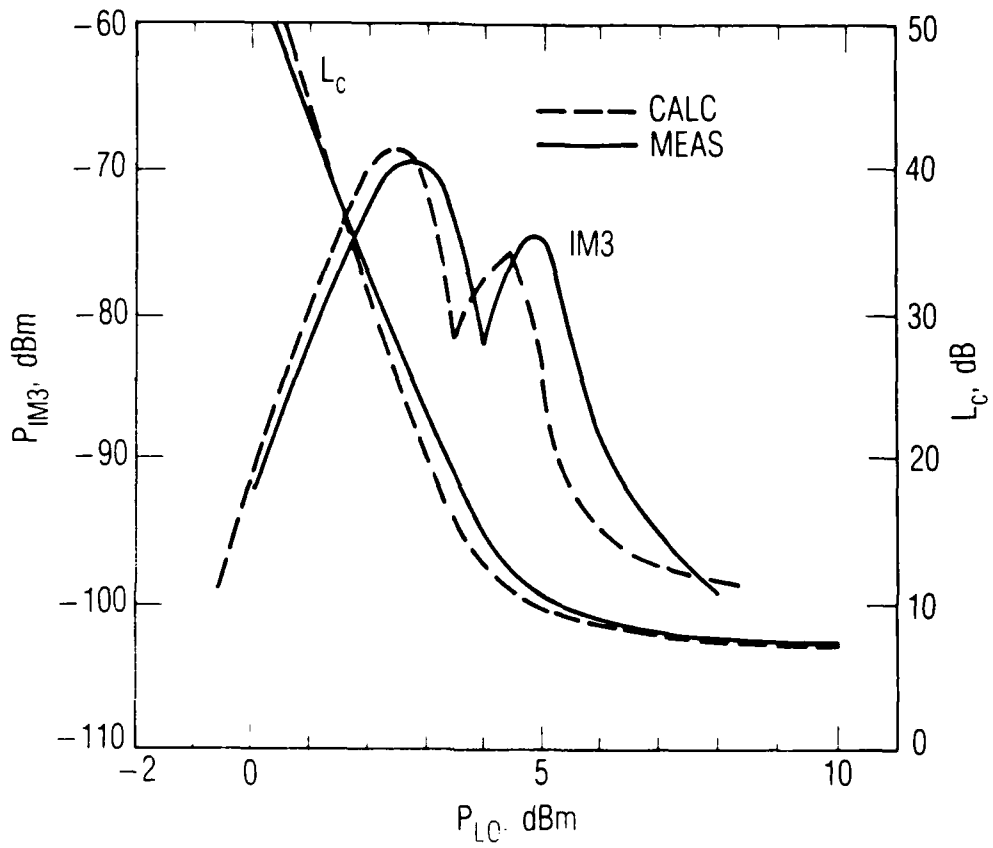


Fig. 5. Measured (solid line) and calculated (dashed line) conversion loss and third-order IM output levels for -20 dBm RF input per tone.  $V_b=0$ .

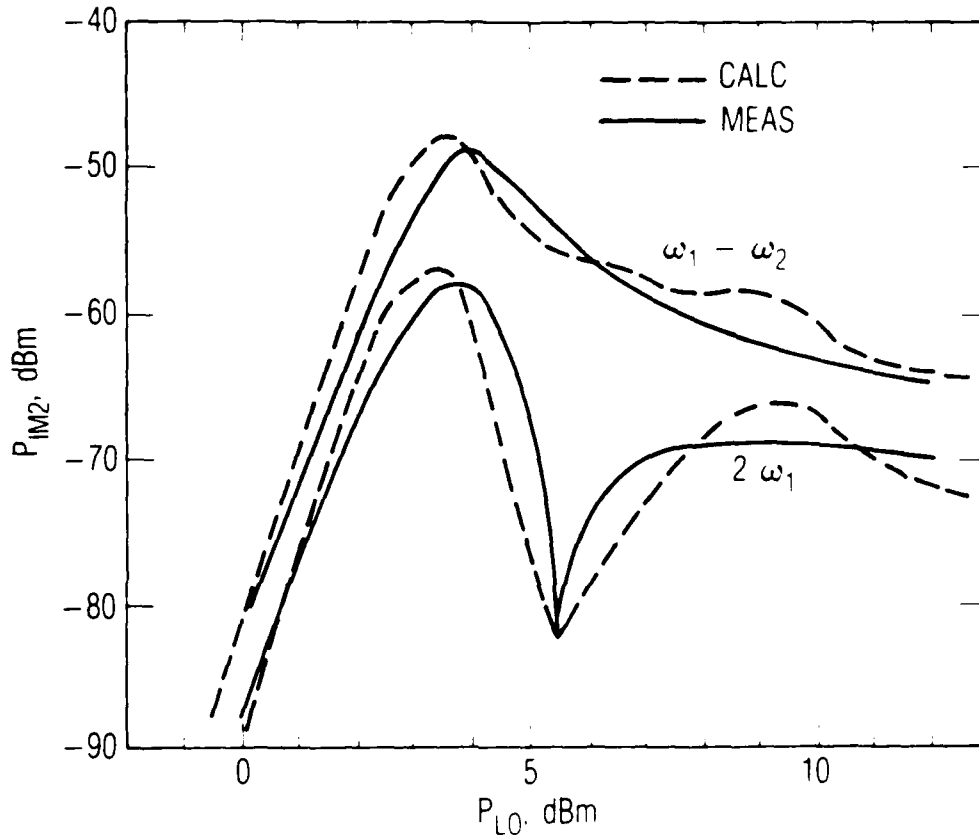


Fig. 6. Measured (solid line) and calculated (dashed line) second-order IM output levels for -20 dBm RF input per tone.  $V_b=0$ .

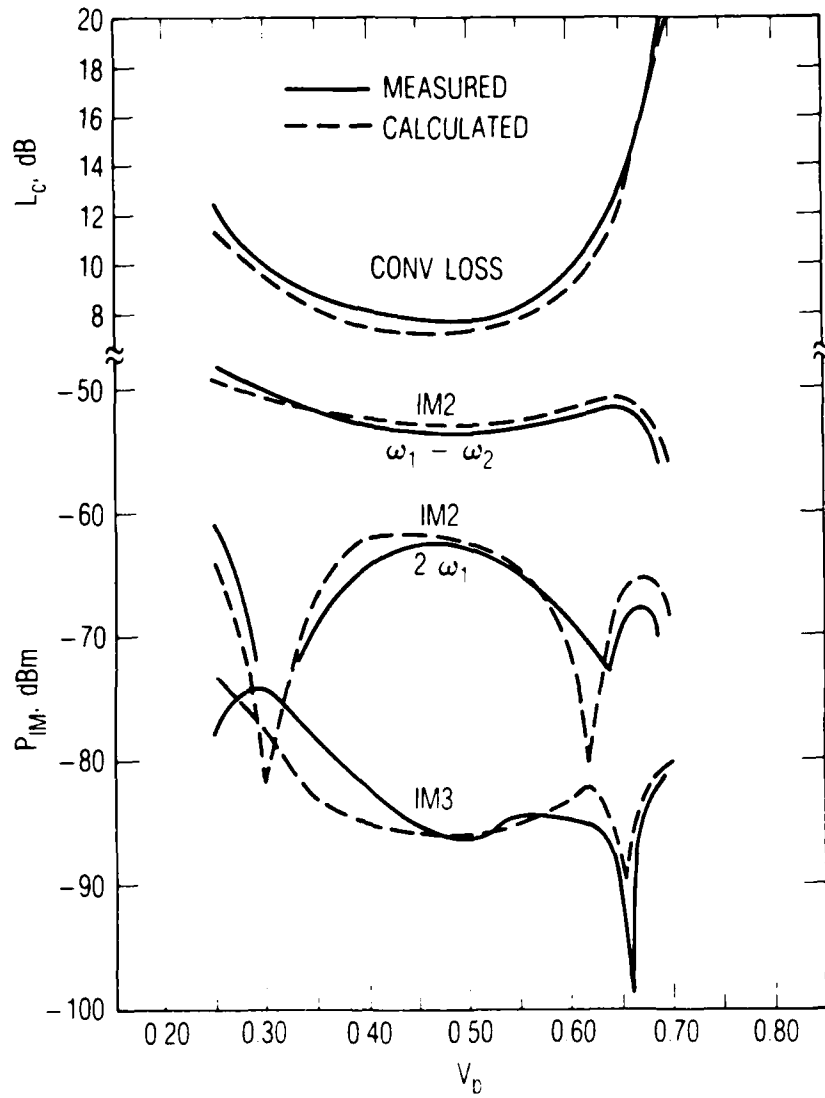


Fig. 7. Measured (solid line) and calculated (dashed line) conversion loss and IM levels as a function of dc bias voltage. LO power is 0 dBm, RF power is -20 dBm per tone.

Figure 8 shows the calculated conversion loss and third-order IM level, for short-circuit and open-circuit high-order small-signal and LO embedding impedances. Also shown are the same data with 50 ohm LO embedding impedances. Figure 9 shows the second-order IM levels under the same conditions. The drop in IM level with increased LO power shown in Figures 5-9 is contrary to intuition, because the LO voltage traverses a progressively more strongly nonlinear range of the I/V and C/V characteristics. The reason is that at high LO levels the junction operates more like a switch than a continuous nonlinearity, and IM current is generated only during the transition between reverse bias and hard forward conduction. This transition becomes shorter as LO power is increased. Similarly, operating the mixer in any way that reduces the length of this transition will reduce intermodulation levels.

The effect of different embedding impedances on the IM level can be related to the interplay of two phenomena. The matrix term in (40) is small for large values of  $Z_{e3}$ , indicating that IM output current should be small. However, the magnitudes of the junction voltage components,  $V_{m,q}$  are relatively large and many may be significant, increasing the magnitudes of the components of the current vector,  $I_3$ , in Eq. (39). The net effect is that the IM levels for short-circuit and open-circuit embedding impedances are comparable at low LO levels, but at high levels the IM output power rises. Furthermore, if the LO source impedance is high,  $C_j$  must discharge through a high impedance during the negative-going half of the LO cycle. This slows the transition between conduction and turn-off, and consequently increases IM levels. Hence it appears that the best possible IM performance



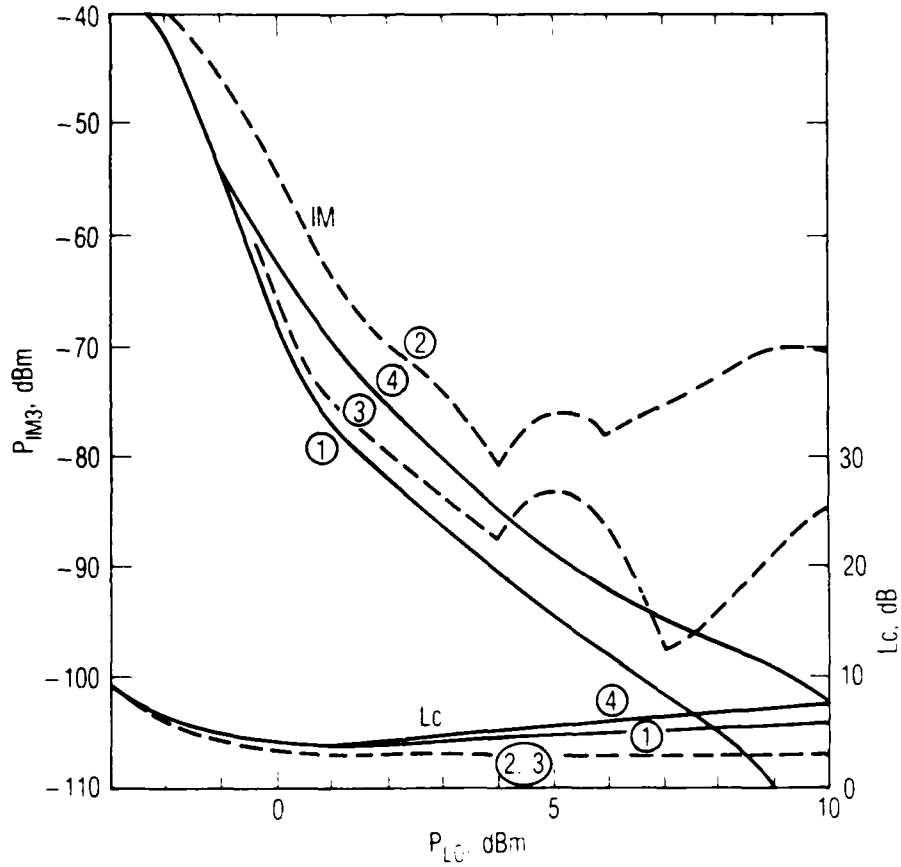


Fig. 8. Conjugate-match conversion loss and third-order IM for baseline diode and circuit parameters, except for different sets of high-order LO and small-signal (including image) embedding impedances: (1)  $Z_e, Z_{LO}$  short circuit; (2)  $Z_e, Z_{LO}$  open circuit; (3)  $Z_e$  open circuit,  $Z_{LO}=50+j0$ ; (4)  $Z_e$  short circuit,  $Z_{LO}=50+j0$ . The LO fundamental embedding impedance is  $50+j0$ . Conversion losses for (2) and (3) are virtually identical.

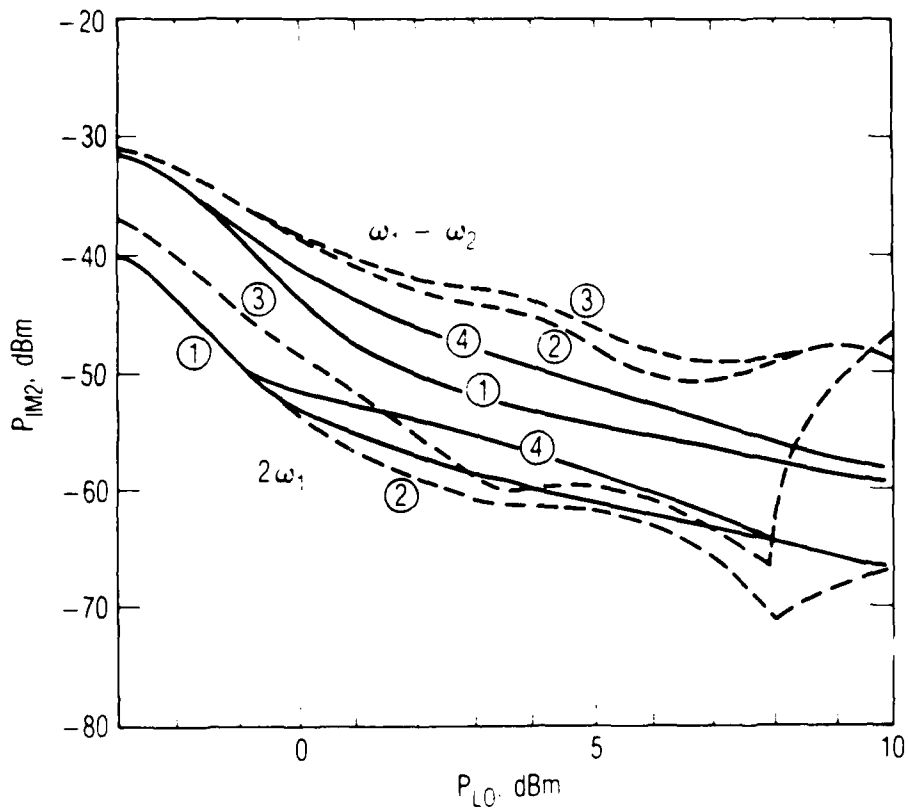


Fig. 9. Second-order IM output levels for the same conditions as in Figure 8

is achieved with short-circuit embedding impedances and heavy LO pumping.

The variation in IM level with LO level in many cases has multiple nulls. This phenomenon is a manifestation of the fact that the excitation currents in Figure 4(b) and 4(c) are not a single sinusoid, but a spectrum of components, related in phase, each downconverted to the same IF. These IF current components experience phase cancellation at certain LO levels. This phenomenon is sensitive in some degree to virtually all mixer and diode parameters, so it is questionable whether it can be used in practice to reduce IM levels significantly.

Figure 10 shows the effect of image enhancement upon IM level, noise temperature, and conversion loss by varying the value of a purely reactive image termination. The termination which gives minimum conversion loss results in a remarkably high noise temperature, a modest rise in second-order IM level, and an enormous rise in third-order IM. Part of the reason for this rise is the high value of IF load impedance,  $600 \Omega$ , necessary to achieve a simultaneous conjugate match at this value of image reactance. It is clear that the best overall performance for this mixer is achieved with a capacitive termination or a short circuit. This phenomenon--low conversion loss accompanied by high noise--is often observed experimentally. It is sobering to note that it may also be accompanied by very poor IM performance.

In Figure 11,  $L_c$  and the IM level are graphed as functions of dc diode current, for fixed bias with the LO level varied, and two fixed LO levels

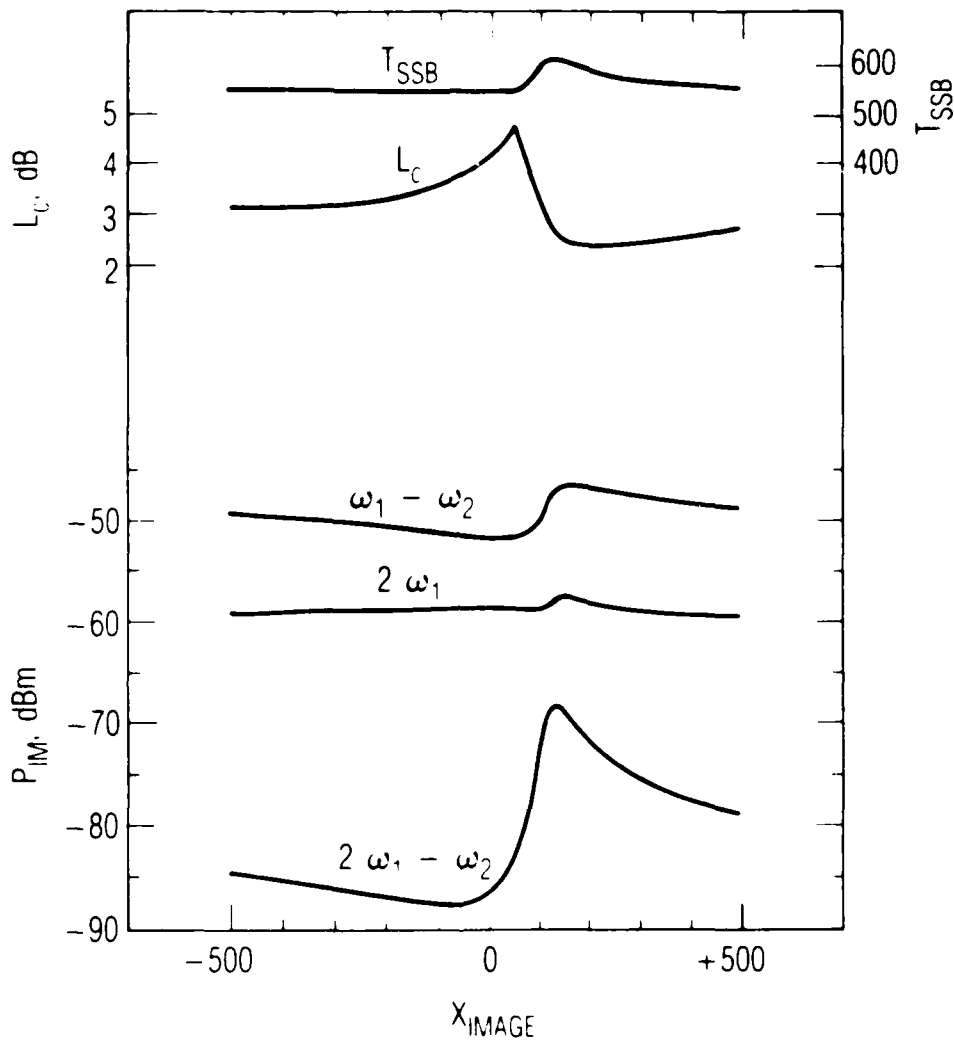


Fig. 10. Conjugate-match conversion loss, IM levels, and noise temperature as a function of image termination reactance, for baseline diode and circuit parameters. All LO and small-signal high-order embedding impedances, except for the image, are zero.  $P_{LO}=3$  dBm,  $V_b=0$ .

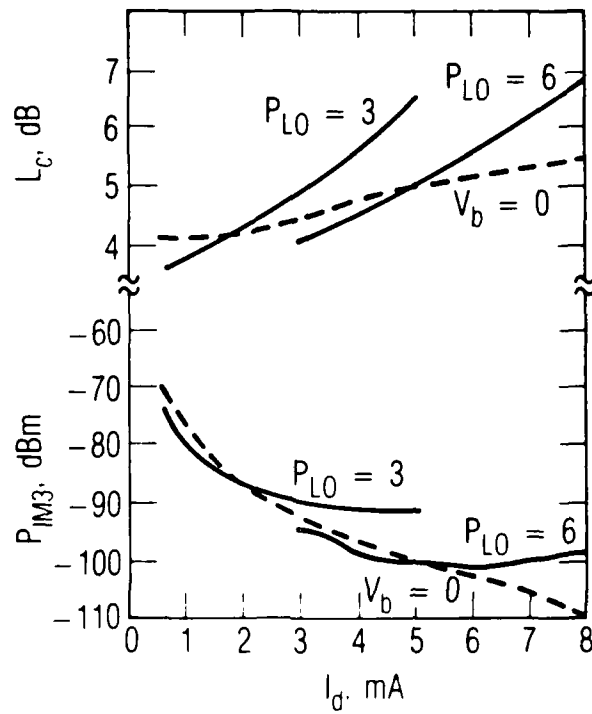


Fig. 11. Conversion loss and IM level vs. dc diode current for fixed LO power and fixed bias voltage conditions, and baseline circuit parameters

with the dc bias varied from -0.2 to 0.3 V. The curves for fixed  $P_{LO}$  and fixed  $V_b$  overlap over wide ranges, but the conversion loss is somewhat better for fixed bias. This remarkable result is due to the fact that the transition regions in the LO waveform vary nearly identically as either bias voltage or LO level is increased.  $L_c$ , however, is affected most strongly by the shape of the conductance waveform, which varies differently with bias and LO level. These results imply that in some cases dc bias can be traded for LO power in order to minimize IM levels.

Figs. 12 and 13 show the dependence of third-order IM upon diode series resistance and junction capacitance, respectively, for three LO power levels. In all cases, the dependence on LO level is stronger than that on diode parameters. Nevertheless, at the high end of the LO range, a low series resistance and low junction capacitance are clearly advantageous.  $C_{j0}$  has a remarkably strong effect on IM level, even though its nonlinearity is relatively weak and it generates little IM current by itself. Its significance comes from its effect on the LO waveform: a low junction capacitance discharges rapidly, allowing the junction voltage to drop through the conduction/nonconduction transition rapidly. Generally, low  $R_s$  results in low IM. The rise in IM level for very low  $R_s$  at high LO levels may be related to the fact that this mixer is conditionally stable at some LO levels for  $R_s < 4\Omega$ . Most real mixers would probably have enough loss in their embedding networks to prevent instability, so this phenomenon might not be observed in practice. Minimizing  $R_s$  is consistent with the need to minimize all embedding impedances.

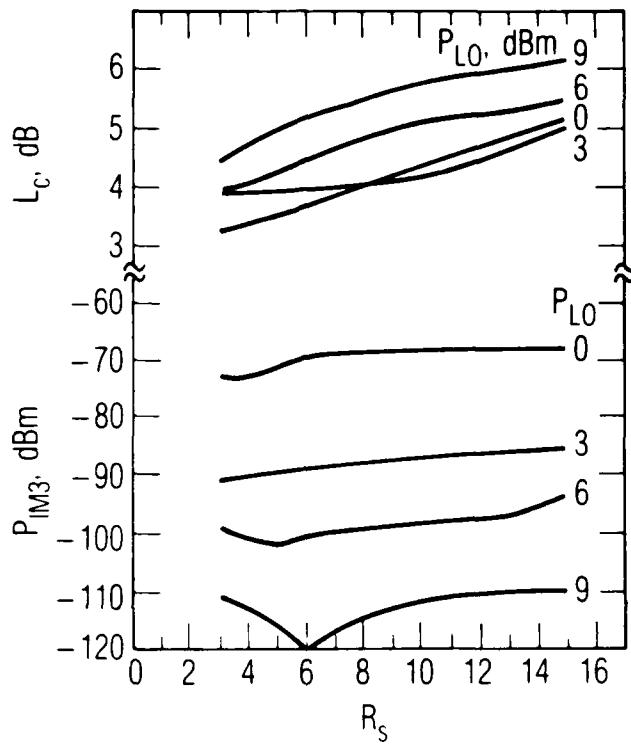


Fig. 12. Conversion loss and IM level dependence on series resistance

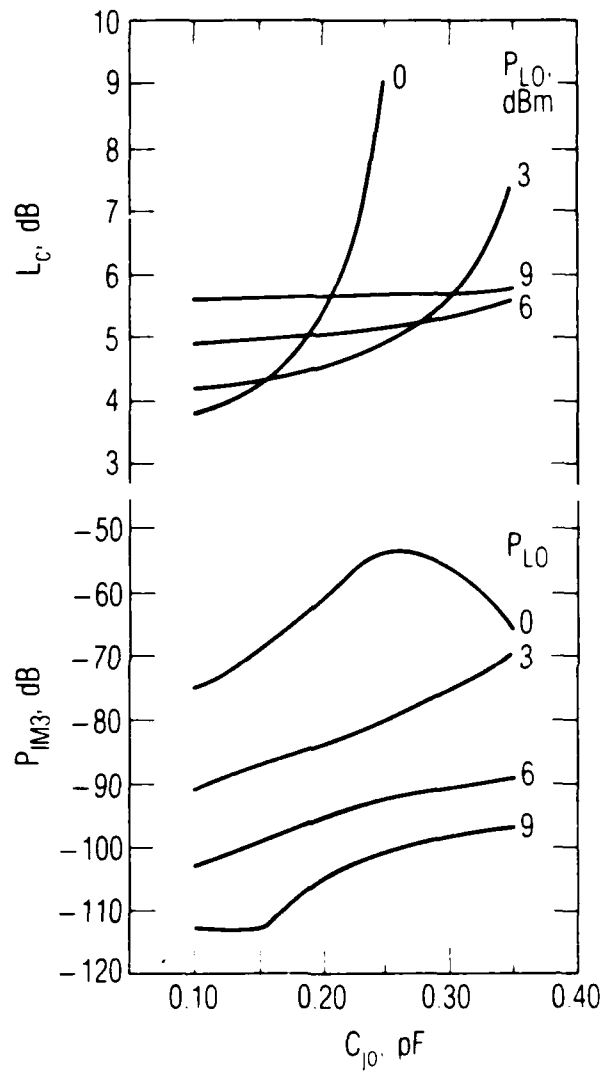


Fig. 13. Conversion loss and IM level dependence on zero-voltage junction capacitance



Figure 14 shows the dependence of IM level upon  $\phi$  and  $\eta$ . Setting  $\phi$  to a large value removes the variation of junction capacitance, and therefore approximates a Mott diode. This change reduces IM level slightly, probably by minimizing the peak value of  $C_j(t)$ . Minimizing  $\eta$  also minimizes IM levels. The drop in conversion loss with increase in  $\eta$  may be surprising. For a conjugate-matched diode, conversion loss rises with LO power above the optimum LO level, in this case 0 dBm, because the junction conductance pulse is longer than optimum. Low  $\eta$  gives a longer conductance pulse, for a given LO level, than does high  $\eta$ . Therefore, the mixer achieves a given value of conversion loss at a lower LO level for low  $\eta$  than high. The noise temperature is, as one might expect, significantly lower for low  $\eta$  than for high  $\eta$ .

#### Conclusions

This report has shown that intermodulation in diode mixers can be predicted with high accuracy. Intermodulation is most strongly related to the speed of the diode's transition between hard conduction and nonconduction, the magnitudes of its junction voltage IM components, and the magnitude of its embedding impedances. The results indicate that the most significant parameter affecting mixer IM performance is LO level. However, high LO level alone is not sufficient to achieve low intermodulation; it is necessary to optimize all mixer diode and circuit parameters. The best IM performance is obtained by using a high-quality diode with low junction capacitance and series resistance. Embedding impedances should be short circuits, and dc bias should be used. Image enhancement must be used with care.

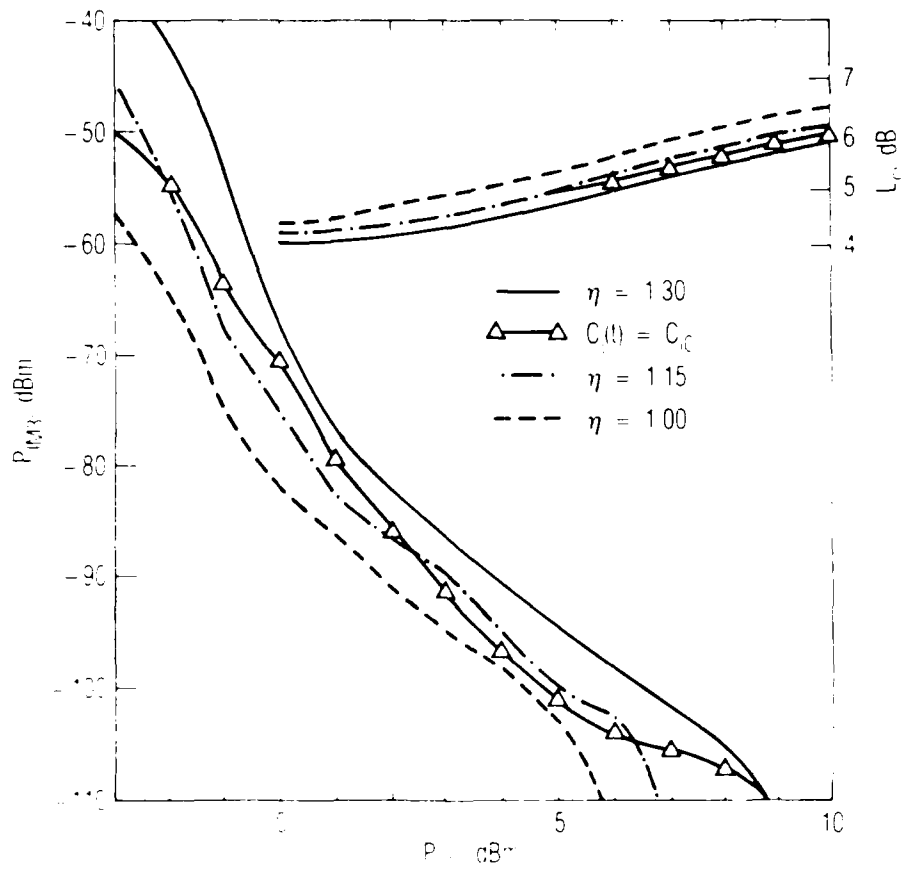


Fig. 14. Conversion loss and IM level dependence on  $\phi$  and  $\eta$

## References

1. E. F. Beane, "Prediction of Mixer Intermodulation Levels as Function of Local Oscillator Power Level" IEEE Trans. Electromagnetic Compatibility, vol. EMC-13, pp. 56-63, May, 1971.
2. J. W. Graham, L. Ehrman, "Nonlinear Systems Modeling and Analysis with Applications to Communications Receivers" Rome Air Dev. Ctr. Tech. Rpt., no. RADC-TR-73-178.
3. J. H. Lepoff, A. M. Cowley, "Improved Intermodulation Rejection in Mixers" IEEE Trans. Microwave Theory Tech., vol. MTT-14, no. 12, pp. 618-23, Dec., 1966.
4. C. P. Tou and B. C. Chang, "A Technique for Intermodulation Reduction in Mixers" IEEE Symp. on Electromagnetic Compatibility, Digest of Papers, pp. 128-132, 1981.
5. A. Ushida, L. O. Chua, "Frequency-Domain Analysis of Nonlinear Circuits Driven by Multi-Tone Signals" IEEE Trans. Circuits and Systems, vol. CAS-31, no. 9, pp. 766-779, Sept., 1984.
6. L. M. Orloff, "Intermodulation Analysis of Crystal Mixer" Proc. IEEE, vol. 52, pp. 173-9, Feb. 1964.
7. R. B. Swerdlow, "Analysis of Intermodulation Noise in Frequency

Converters by Volterra Series" IEEE Trans. Microwave Theory Tech., vol. MTT-26, no. 4, pp. 305-13, April, 1978.

8. E. N. Gusinskiy, L. M. Kushnir, N. V. Soina, "The Level of Intermodulation and Combination Interference in a Diode Mixer" Telecomm. and Radio Engineering, vol. 32, no. 5, pp. 127-9, May, 1977.

9. L. M. Kushnir, V. V. Soina, M. S. Fogel'son, E. N. Gusinskiy, "Influence of Diode and Load Parameters on Intermodulation Noise Supression in a Diode Mixer" Telecomm. and Radio Engineering, vol. 33, no. 3, pp. 118-20, March, 1978.

10. J. G. Gardiner, A. M. Yousif, "Distortion Performance of Single-Balanced Diode Modulators" Proc. IEE, vol. 117, no. 8, pp.1609-14, Aug., 1970.

11. D. N. Held, A. R. Kerr, "Conversion Loss and Noise of Microwave and Millimeter-Wave Mixers: Part 1-Theory; Part 2-Experiment" IEEE Trans. Microwave Theory Tech., vol. MTT-26, no. 2, pp. 49-61, Feb., 1978.

12. S. A. Maas, Microwave Mixers, Artech House, Dedham, MA, 1986.

13 A. R. Kerr, "A Technique for Determining the Local Oscillator Waveforms in a Microwave Mixer" IEEE Trans. Microwave Theory Tech., vol. MTT-23, no. 10, pp. 828-31, Oct., 1975.

14. Borland International, 4113 Scotts Valley Dr., Scotts Valley, CA 95066.

15. S. Maas, "An Interactive Microwave Mixer Analysis Program" Aerospace Corp. Technical Report no. TR-0086(692502)-8, 1986.

## LABORATORY OPERATIONS

The Aerospace Corporation functions as an "architect-engineer" for national security projects, specializing in advanced military space systems. Providing research support, the corporation's Laboratory Operations conducts experimental and theoretical investigations that focus on the application of scientific and technical advances to such systems. Vital to the success of these investigations is the technical staff's wide-ranging expertise and its ability to stay current with new developments. This expertise is enhanced by a research program aimed at dealing with the many problems associated with rapidly evolving space systems. Contributing their capabilities to the research effort are these individual laboratories:

Aerophysics Laboratory: Launch vehicle and reentry fluid mechanics, heat transfer and flight dynamics; chemical and electric propulsion, propellant chemistry, chemical dynamics, environmental chemistry, trace detection; spacecraft structural mechanics, contamination, thermal and structural control; high temperature thermomechanics, gas kinetics and radiation; cw and pulsed chemical and excimer laser development including chemical kinetics, spectroscopy, optical resonators, beam control, atmospheric propagation, laser effects and countermeasures.

Chemistry and Physics Laboratory: Atmospheric chemical reactions, atmospheric optics, light scattering, state-specific chemical reactions and radiative signatures of missile plumes, sensor out-of-field-of-view rejection, applied laser spectroscopy, laser chemistry, laser optoelectronics, solar cell physics, battery electrochemistry, space vacuum and radiation effects on materials, lubrication and surface phenomena, thermionic emission, photo-sensitive materials and detectors, atomic frequency standards, and environmental chemistry.

Computer Science Laboratory: Program verification, program translation, performance-sensitive system design, distributed architectures for spaceborne computers, fault-tolerant computer systems, artificial intelligence, microelectronics applications, communication protocols, and computer security.

Electronics Research Laboratory: Microelectronics, solid-state device physics, compound semiconductors, radiation hardening; electro-optics, quantum electronics, solid-state lasers, optical propagation and communications; microwave semiconductor devices, microwave/millimeter wave measurements, diagnostics and radiometry, microwave/millimeter wave thermionic devices; atomic time and frequency standards; antennas, rf systems, electromagnetic propagation phenomena, space communication systems.

Materials Sciences Laboratory: Development of new materials: metals, alloys, ceramics, polymers and their composites, and new forms of carbon; non-destructive evaluation, component failure analysis and reliability; fracture mechanics and stress corrosion; analysis and evaluation of materials at cryogenic and elevated temperatures as well as in space and enemy-induced environments.

Space Sciences Laboratory: Magnetospheric, auroral and cosmic ray physics, wave-particle interactions, magnetospheric plasma waves; atmospheric and ionospheric physics, density and composition of the upper atmosphere, remote sensing using atmospheric radiation, solar physics, infrared astronomy, infrared signature analysis; effects of solar activity, magnetic storms and nuclear explosions on the earth's atmosphere, ionosphere and magnetosphere; effects of electromagnetic and particulate radiations on space systems; space instrumentation.

END

5-87

DTIC